Structure and Properties of New Thermoforming Bionanocomposites Based on Chitin Whisker-Graft-Polycaprolactone

6 AUTHORS, INCLUDING:

Alain Dufresne
Grenoble Institute of Technology
312 PUBLICATIONS 15,283 CITATIONS

SEE PROFILE

Jin Huang
KTH Royal Institute of Technology
152 PUBLICATIONS 2,339 CITATIONS

SEE PROFILE

Structure and Properties of New Thermoforming Bionanocomposites Based on Chitin Whisker-*Graft*-Polycaprolactone

Liangdong Feng,[1] Ziyan Zhou,[2] Alain Dufresne,[3] Jin Huang,[2,3] Ming Wei,[2] Lijia An[4]

[1]Key Laboratory of Attapulgite Science and Applied Technology of Jiangsu Province, Department of Chemical Engineering, Huaiyin Institute of Technology, Huai'an 223003, China
[2]College of Chemical Engineering, Wuhan University of Technology, Wuhan 430070, China
[3]Ecole Francaise de Papeterie et des Industries Graphiques, Institut National Polytechnique de Grenoble (EFPG-INPG) BP65, 38402 Saint-Martin d'Héres Cédex, France
[4]State Key Laboratory of Polymer Physics and Chemistry, Changchun Institute of Applied Chemistry, Chinese Academy of Sciences, Changchun 130022, China

ABSTRACT: Thermoformable bionanocomposites of chitin whisker-*graft*-polycaprolactone (CHW-*g*-PCL) were synthesized by initiating the ring-opening polymerization of caprolactone monomer onto the CHW surface under microwave radiation. In this case, the "graft from" strategy contributed to long and dense "plasticizing" PCL tails onto the CHW surface as the key of thermoforming, and, therefore, such bionanocomposites were injection-molded as the sheets with a structure of cocontinuous phase mediated with the entanglement of grafted PCL chains. The structure and properties of the molded CHW-*g*-PCL sheets were investigated by FTIR, XRD, SEM, DSC, DMTA, contact angle measurement, and tensile test. With an increase of the PCL content in CHW-*g*-PCL, the strength and elongation as well as the hydrophobicity of the nanocomposites increased at one time. This is the first report on the thermoformable polymer-grafted nanocrystal derived from natural polysaccharide. Moreover, such new bionanocomposites with good mechanical performances could have great potential applications. © 2009 Wiley Periodicals, Inc. J Appl Polym Sci 112: 2830–2837, 2009

Key words: chitin whisker; bionanocomposite; graft; thermoforming; mechanical properties

INTRODUCTION

Natural polymers from renewable resources exhibit the advantages of biodegradability, biocompatibility, nontoxicity, high reactivity, low cost, easy-to-avail-

ability, and so on, and hence have been used as excellent raw substances in the field of materials for saving fossil resources and protecting environment.[1–3] Born out of the growing interest in predominant performances of nanocomposites attributed to nanofillers, a kind of novel nanomaterials derived from natural polymers, named as "green" bionanocomposites,[4,5] has been emerging, in which natural polymers can act as the matrix, the nanofiller, or both. Meanwhile, the crystalline components extracted from natural polysaccharides are rigid nano-objects with a uniform structure, and are so-called rod-like whiskers of cellulose[6] and chitin,[7] and platelet-like nanocrystal of starch.[8,9] These nanocrystals as popular natural nanofiller for the bionanocomposites not only inherit all the virtues of natural polymers, but also show a reinforcing function similar to the traditional inorganic nanofillers.[6,7,10–12] In addition, a active surface of natural nanofillers facilitates chemical derivation[13,14] and grafting,[15–17] and forms strong physical interaction with polymer matrix.[6] So far, the cellulose and chitin whiskers as well as starch nanocrystal have been used to reinforce many natural and synthetic polymeric materials, such as natural

rubber,[6,11,18] polypropylene,[19,20] poly(vinyl chloride),[21] poly(vinyl acetate),[22] poly(ethylene-co-vinyl acetate),[23] poly(styrene-co-butyl acrylate),[24] waterborne epoxy,[25,26] poly(oxyethylene),[27] waterborne polyurethane,[28,29] poly(β-hydroxyoctanoate),[30,31] poly(lactic acid),[32,33] polycaprolactone,[34] silk fibroin,[35] cellulose acetate butyrate,[36] starch[10,37] and soy protein,[38–40] plastics, etc.

Same as other traditional nanoparticles, natural nanocrystals are easy to self-aggregate as well and even form the agglomerates in micrometer scale. The self-aggregation inhibits the positive function of natural nanocrystals in nanocomposites. Additionally, because the polar hydroxyl groups are near the surface of nanocrystal, the forming of interfacial interaction with polymer matrix is also inhibited. Furthermore, the hydroxyl groups onto the surface of nanocrystal might be immiscible with hydrophobic polymer matrix. As a result, it is essential for the surface chemical modification of natural nanocrystals based on the reactivity of hydroxyl groups on its surface.[13–17] As reported, surface chemical modification improves the dispersion of starch nanocrystal in nanometer scale,[14–16] manipulates the hydrophobicity of surface,[13–16] and enhances the miscibility between nanocrystal and polymer matrix. Especially, chemical grafting resulted in the long tails on the surface of nanocrystal, which might penetrate into polymer matrix to enhance the miscibility of nanocrystal and matrix and the reinforcing role of nanocrystal mediated with strong interfacial interaction. Furthermore, the plasticizing of the grafted long tails can contribute to thermoforming of nanocrystal-based bionanocomposites. Depending on the entanglement of grafted polymer chains, the resultant materials show a structure of cocontinuous phase.[16]

In this work, the surface of chitin whisker (CHW) was functionalized by grafting polycaprolactone (PCL) chains based on "graft from" strategy. The "graft from" strategy dissolved a key issue of thermoforming, namely long and dense "plasticizing" tails of PCL formed onto the CHW surface. Subsequently, the PCL grafted CHW was attempted to injection mold as sheets. On the basis of the rigidity of CHW and the cocontinuous structure mediated with the entangling of grafted PCL chains, high mechanical performances were expected. Meanwhile, a great amount of PCL in modified CHW was possible to enhance water-resistance. At last, the structure and properties of resultant bionanocomposite materials were investigated by Fourier transform infrared spectroscopy (FTIR), X-ray diffraction (XRD), differential scanning calorimetry (DSC), dynamic mechanical analysis (DMA), scanning electron microscope (SEM), contact angle measurement, and tensile test. Moreover, the role of "plasticizing" grafted PCL tails were discussed.

EXPERIMENTAL

Materials

Chitin from crab shells was supplied by Yuhuan Sea Biochemical Co. (Zhejiang, China). ε-Caprolactone (CL) monomer (99%) was purchased from Alfa Aesar and used as received. Tin(II) octoate (Sn(Oct)$_2$) and other reagents of analytical grade were purchased from the Shanghai Sinopharm Chemical Co. (Shanghai, China), and used as received.

Extraction of chitin whiskers (CHWs)

The chitin whiskers were extracted according to previous report.[41] The commercial chitin powder was dispersed into a 5 wt % KOH aqueous solution, and then boiled for 6 h under mechanical stirring to remove most proteins. The resultant suspension was conditioned at ambient temperature overnight under mechanical stirring followed by filtering and washing with distilled water for several times. Subsequently, the crude product was bleached with 17 g of NaClO$_2$ in 1 L of water containing 0.3M sodium acetate buffer for 6 h at 80°C, and then fully rinsed with distilled water. Thereafter, the crude product was dispersed into a 5 wt % KOH aqueous solution for 48 h to remove residual proteins followed by centrifuging to produce protein-free chitin. 1 g of protein-free chitin was hydrolyzed with 30 mL 3M HCl at the boiling point for 90 min under mechanical stirring. After acid hydrolysis, the suspension was diluted with distilled water and then centrifuged for three times to produce protein-free CHW. The resultant chitin whiskers were dialyzed in distilled water until a pH was ~ 4. At last, the CHWs were dispersed into water by ultrasonic treatment followed by lyophilizing as loose powders.

Preparation and thermoforming of CHW-g-PCL

The mixtures of loose CHW powder and CL monomer with the given weight ratios of 1 : 70, 1 : 90, and 1 : 100 were placed into an ampoule, respectively. Subsequently, the catalyst of Sn(Oct)$_2$ was added, whose weight was 0.5% of the CL weight. The mixture was homogenized by Lab Dancer (IKA), and then vacuum-exhausted for 30 min. Thereafter, the ampoule containing reactant was conditioned under a microwave irradiation of 255 W power for 3 min. At last, the crude product was dissolved by CH$_2$Cl$_2$ followed by precipitating with methanol. This process of purification was carried out for many times to remove monomer, catalyst and homopolymer. In this stage, the removing of homopolymer is a key issue. Considering that the chitin whisker-graft-polycaprolactone (CHW-g-PCL) is more easily precipitated than homopolymer due

to the poor solubility of the CHW component in CH_2Cl_2 and a greater PCL fraction in the CHW-*g*-PCL, the classification method in every precipitation process was used to collect the initial precipitate.[42] Meanwhile, FTIR was used to trace every precipitate until the relative intensity of $-C=O$ peak assigned to PCL was almost invariable. The purified products were vacuum-dried, and coded as CHW-*g*-PCL(I) (1 : 70), CHW-*g*-PCL(II) (1 : 90), and CHW-*g*-PCL(III) (1 : 100), respectively, according to the feeding weight ratio of CHW versus CL listed in bracket.

The inject-molding of the resultant CHW-*g*-PCL nanocomposites was carried out on a micro-injection molding machine (Thermo Electron Corp., USA). The temperature, time, and pressure of injection were 65°C, 20 s, and 0.55 MPa, respectively, while the mold temperature was 40°C.

Characterization

Element analysis of the CHW-*g*-PCL and CHW powders was measured on Vario EL III elemental analyzer (Elementar, Germany).

FTIR spectra of the CHW, and CHW-*g*-PCL powders as well as all the sheets were also recoded on a FTIR 5700 spectrometer (Nicolet, USA). The powders were measured by a KBr-pellet method in the range from 4000 cm^{-1} to 400 cm^{-1}, and the sheets were scanned by using Smart OMNT reflect accessories in the range from 4000 cm^{-1} to 700 cm^{-1}.

XRD measurements were performed on a D/max-2500 X-ray diffractometer (Rigaku Denki, Japan) with Cu Kα_1 radiation ($\lambda = 0.154$ nm) in a range of $2\theta = 3$–$60°$ using a fixed time mode with a step interval of $0.02°$.

SEM observation was carried out on an *S*-3000*N* scanning electron microscope (Hitachi, Japan). The sheets were frozen in liquid nitrogen and then snapped immediately. The fractured surfaces of the sheets were sputtered with gold, and then observed and photographed.

TEM observation was carried out on an H-7000FA electron microscope (Hitachi, Japan) at 75 kV. In the process of preparing CHW, the CHW suspension dispersed by ultrasonic treatment was directly used. In addition, the CHW-*g*-PCL was dissolved in CH_2Cl_2, and then dispersed in distilled water followed by rotating evaporation to remove CH_2Cl_2. The suspensions of CHW and CHW-*g*-PCL were respectively, diluted as a concentration of ~ 0.5 wt %, and then negatively stained with 2% (w/v) aqueous solution of uranyl acetate.

DSC was carried out on a DSC-Q200 instrument (TA Instruments, USA) under nitrogen atmosphere at a heating or cooling rate of 20°C min^{-1}. The sheets were scanned in the range from -90 to 200°C after a

pretreatment (heating from 20 to 100°C and then cooling down to $-90°$C) of eliminating thermal history.

DMA was carried out on a DMA 242C dynamic mechanical analyzer (Netzsch, Germany) at a frequency of 1 Hz. The temperature ranged from $-150°$C to 100°C with a heating rate of 3°C min^{-1}. Measurements were performed using a dual cantilever device and the size of the testing samples was 40 $\times$10 mm^2.

Contact angle measurements of water on the CHW-*g*-PCL surface were performed at room temperature using a DSA100 contact angle analyser (Kruss, Germany). Furthermore, the mixing solution, composed of various weight ratio of glycol versus water, with differing dispersive and polar surface tensions were used to determine the total surface energy (γ^{total}) of the CHW-*g*-PCL sheets with various CHW content.

The tensile strength (σ_b), elongation at break (ε_b), and Young's modulus (E) of the CHW-*g*-PCL sheets were measured on a universal testing machine (CMT6503, Shenzhen SANS Test Machine Co., Shenzhen, China) with a tensile rate of 10 mm min^{-1} according to ISO527-3 : 1995(E). The tested samples were kept in the humidity of 35% for 7 days before measurement. An average value of five replicates of each sample was taken.

RESULTS AND DISCUSSION

Structure and composition of CHW-*g*-PCL

FTIR spectra of the CHW-*g*-PCL(III) and CHW powders are depicted in Figure 1. Compared with the spectrum of CHW, the prominent change after grafting process was the appearance of one distinct peak located at 1727.5 cm^{-1} assigned to ester-carbonyl group of grafted PCL chains. It indicated that the PCL and CHW were successfully linked together to
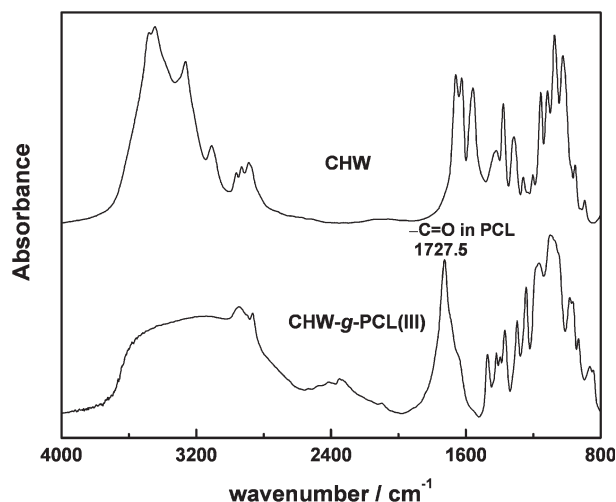

Figure 1 FTIR spectra of the CHW and CHW-*g*-PCL(III) powders, where the CHW-*g*-PCL(III) is used as the representative of grafted CHW.
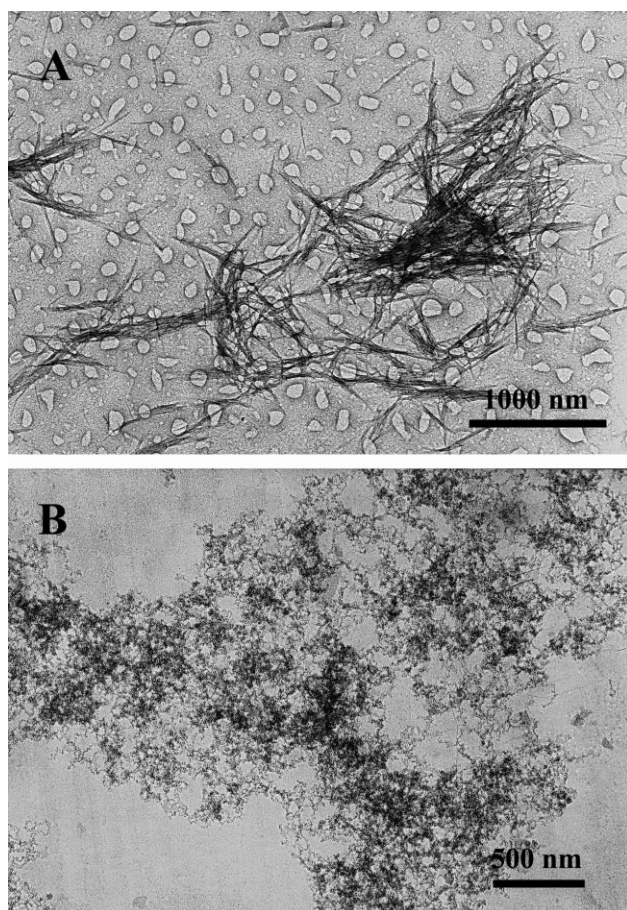
Figure 2 TEM images of the CHW and CHW-*g*-PCL(III) nanoparticles, where the CHW-*g*-PCL(III) is used as the representative of grafted CHW.

produce a kind of new nanoparticles, whose surface was covered with the PCL brush. Furthermore, although the exact number and length of grafted PCL chains was difficult to determine under our great efforts, the PCL content can be calculated by element analysis. The contents of C element in CHW-*g*-PCLs and CHW were determined as 61.01%
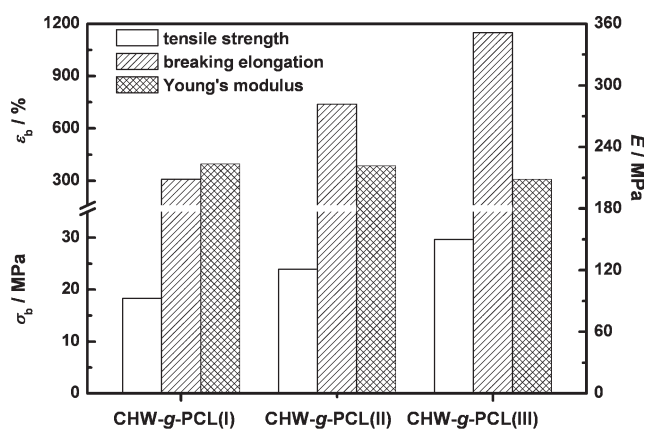

Figure 3 Mechanical properties of the thermoforming CHW-*g*-PCL sheets with various CHW content.
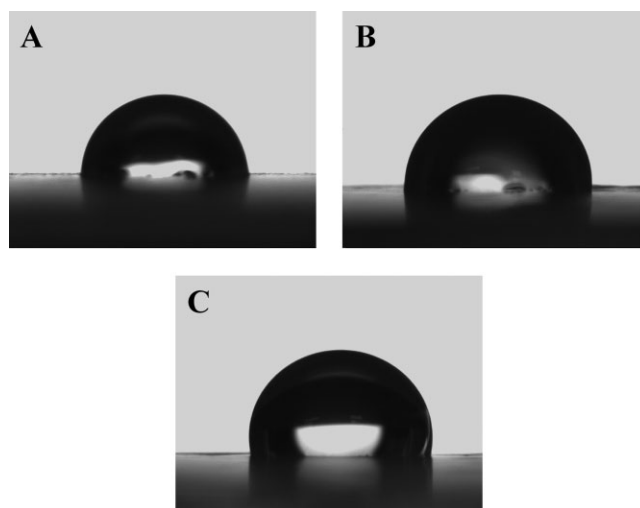

Figure 4 Photographs of a water drop on the surface of thermoforming CHW-*g*-PCL sheets with various CHW content (A: CHW-*g*-PCL(I), B: CHW-*g*-PCL(II), C: CHW-*g*-PCL(III)).

($C_{\text{CHW-}g\text{-PCL(I)}}$), 61.34%($C_{\text{CHW-}g\text{-PCL(II)}}$), 62.08% ($C_{\text{CHW-}g\text{-PCL(III)}}$), and 42.48% ($C_{\text{CHW}}$) by element analysis, respectively, while the content of C element in PCL was fixed as the theoretical value of 63.16% (C_{PCL}). Consequently, the content of grafted PCL chains in CHW-*g*-PCL was calculated by the following equation:

$$x\, C_{\text{PCL}} + (1-x)\, C_{\text{CHW}} = C_{\text{CHW-}g\text{-PCL}} \qquad (1)$$

where x is the weight percentage of grafted PCL chains in CHW-*g*-PCL. The result showed that the grafted PCL contents in CHW-*g*-PCLs were 89.60 wt % of CHW-*g*-PCL(I), 91.20 wt % of CHW-*g*-PCL(II),
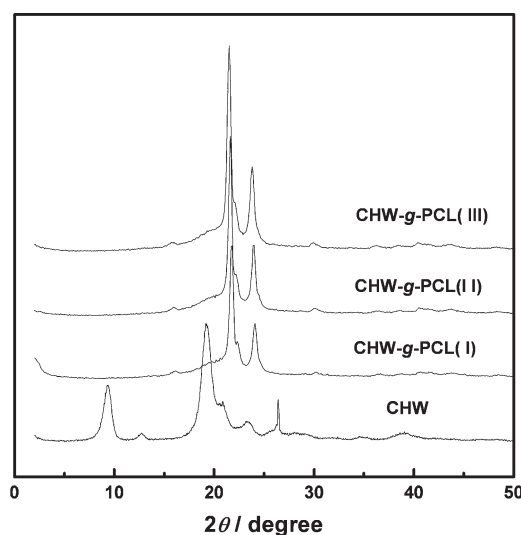

Figure 5 XRD patterns of the thermoforming CHW-*g*-PCL sheets with various CHW content as well as the CHW as reference.
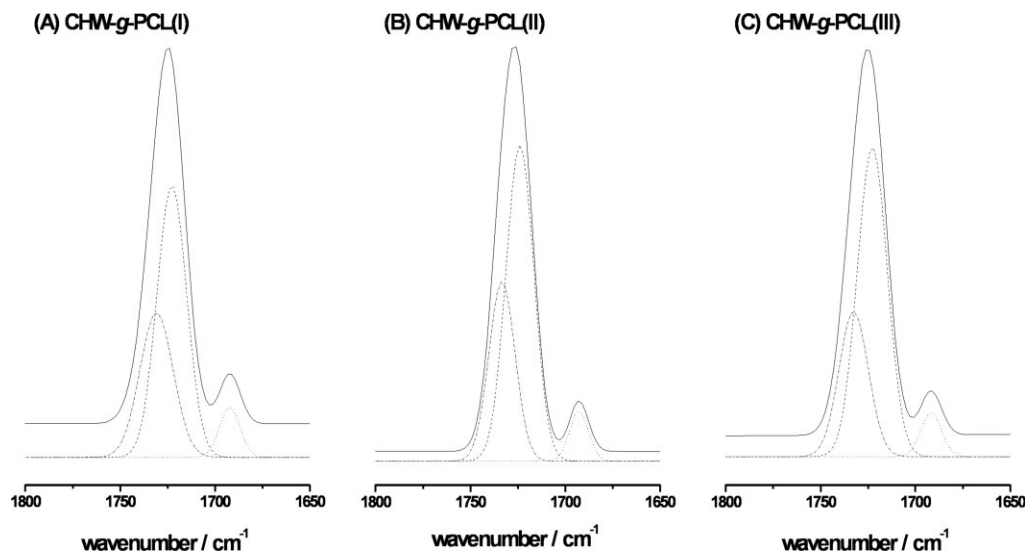
Figure 6 Experimental and curve-fitted FTIR spectra of the thermoforming CHW-g-PCL sheets with various CHW content in the range of 1650–1800 cm^{-1}. (— experimental curve; ----- —C=O in amorphous region; ---- —C=O in crystalline domain; ····· hydrogen-bonded —C=O)

94.78 wt % of CHW-g-PCL(III), indicating that a great component of PCL chains stood onto the CHW-g-PCL nanoparticles.

Same as the previous report,[13] ungrafted CHW whiskers could be identified as the rod-like structure, where the dimension of neat CHW whiskers had a diameter of $\sim$ 20 nm and a length of several hundreds nanometer [seen in Fig. 2(A)]. However, the CHW-g-PCL nanoparticles in Figure 2(B) showed a fluey structure with a length of less than 100 nm. It suggested that the process of grafting PCL chains partly destroyed the original structure of CHW, and hence produced the nano-objects of CHW-g-PCL with smaller size.

Mechanical properties of CHW-g-PCL sheets

Figure 3 shows the mechanical properties of the thermoforming CHW-g-PCL sheets, including tensile strength (σ_b), Young's modulus (E) and elongation

at break (ε_b). With an increase of the PCL content in CHW-g-PCL, the tensile strength and elongation simultaneously enhanced while the Young's modulus slightly decreased. The CHW-g-PCL(III) with the highest PCL content showed the maximum tensile strength of 29.7 MPa and elongation of 1148%. Meanwhile, the grafted PCL chains tended to entangle with each other, and hence facilitated the transferring and split-up of the stress. At this time, the rigid CHW as the concentrated point of the stress could fully play the reinforcing function.

Hydrophobic surface of CHW-g-PCL sheets

The CHW was hydrophilic in nature owing to the hydroxyl groups on the surface. However, the CHW-g-PCL with grafted PCL chains showed a distinct hydrophobicity. As seen in Figure 4, the contact angles of water (θ_{water}) on the CHW-g-PCLs' surfaces were higher than 86°, and the θ_{water} values

TABLE I
Location and Fraction of Curve-Fitting Peaks for the —C=O Absorption in the FTIR Spectra of the CHW-g-PCL Nanocomposites with Various PCL Content

	FTIR data					
	Peak I		Peak II		Peak III	
Sample	Location (cm^{-1})	F_{amorp} (%)	Location (cm^{-1})	F_{crys} (%)	Location (cm^{-1})	$F_{H\text{-}bond}$ (%)
CHW-g-PCL(I)	1730.8	34.55	1722.8	58.01	1692.1	7.44
CHW-g-PCL(II)	1733.4	32.42	1723.9	60.99	1692.7	6.59
CHW-g-PCL(III)	1732.6	29.47	1722.7	64.21	1691.7	6.32

(Peak I: —C=O in Amorphous Region; Peak II: —C=O in Crystalline Domain; Peak III: Hydrogen-Bonded —C=O).

gradually increased with an increase of the PCL content in CHW-g-PCL. The CHW-g-PCL(I) and CHW-g-PCL(II) had the similar θ_{water} values as 86° and 87°, respectively, while the CHW-g-PCL(III) with the highest PCL content showed the maximum θ_{water} as 107°. Meanwhile, the effect of the PCL content on total surface energy (γ^{total}) was the same as that on θ_{water}. The γ^{total} values of CHW-g-PCL(I), CHW-g-PCL(II), and CHW-g-PCL(III) were 35.00 ± 2.34, 35.00 ± 2.51 and 16.45 ± 1.85 mJ m^{-2}, respectively. In conclusion, the grafted PCL chains on the surface of CHW contributed to the hydrophobicity of thermoforming bionanocomposites. Furthermore, higher the PCL content in CHW-g-PCLs was, more hydrophobic the bionanocomposites became.

Structure of CHW-*g*-PCL sheets

XRD patterns of the thermoforming CHW-g-PCL sheets as well as neat CHW powder are depicted in Figure 5. The neat CHW showed two predominant diffractions located at 9.4° and 19.1° of 2θ. However, the characteristic diffraction of CHW submerged into the strong diffraction assigned to grafted PCL chains for the CHW-g-PCL nanocomposites due to low CHW content. All the CHW-g-PCL nanocomposites showed the analogous diffraction patterns, shown as two crystalline peaks located at 21.5° and 23.8° of 2θ. Furthermore, the diffuse character of diffraction peaks of the CHW-g-PCL nanocomposites suggested a semicrystalline character.

In general, the vibration of groups in FTIR spectrum of a semicrystalline polymer should be composed of three components arising from its crystalline and amorphous phases as well as hydrogen bonding. As a result, the stretching vibration of —C=O located at ~ 1727 cm^{-1} assigned to grafted

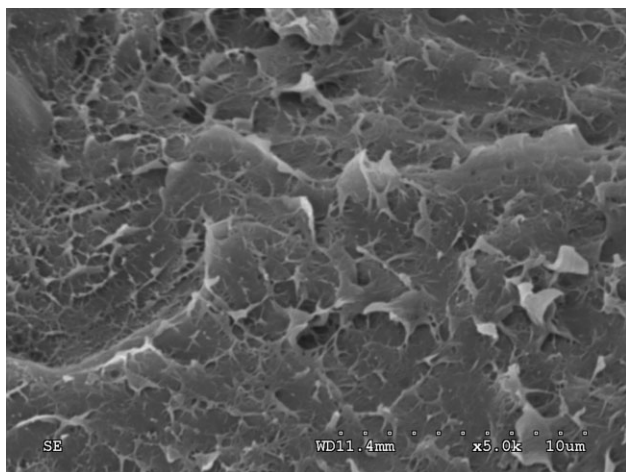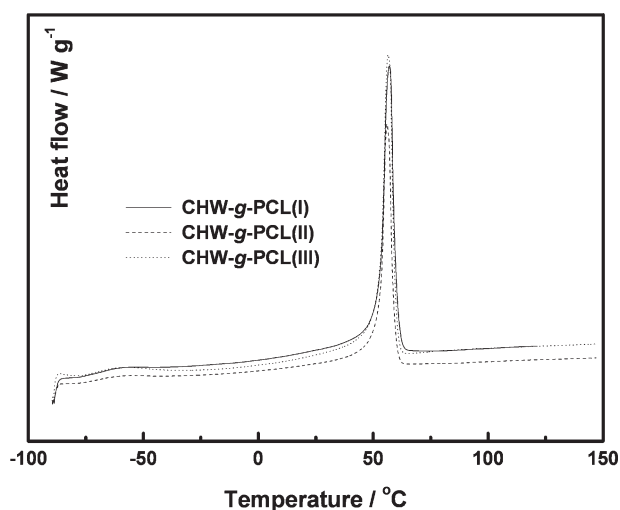**Figure 8** DSC thermograms of the thermoforming CHW-*g*-PCL sheets with various CHW content.

PCL chains was divided into three peaks assigned to the states of crystalline, amorphous and hydrogen bonding by curve-fitting (seen in Fig. 6). The fraction and location of three curve-fitted peaks are summarized in Table I, where the fraction of crystalline peak is proportional to crystalline degree (χ_c). Obviously, with an increase of the PCL content in CHW-*g*-PCL, the fraction of crystalline peaks increased while the fractions of amorphous peaks and hydrogen-bonding peak decreased. As a result, higher crystalline degree was attributed to higher content of grafted PCL chains.

Furthermore, all the CHW-g-PCL nanocomposites had the coarse fractured surface, and the SEM image of CHW-g-PCL(III) as a representative is shown in Figure 7. This kind of characteristic fractured surface indicated that the grafted PCL chains entangled each other, which contributed to great elongation and the transferring of stress to rigid CHW.

Thermal properties of CHW-*g*-PCL sheets

Figure 8 shows the DSC thermograms of the CHW-g-PCL nanocomposites, and the melting temperature (T_m) and heat enthalpy (ΔH_m) assigned to the PCL component are summarized in Table II. The

Figure 7 SEM image of fractured surface for the thermoforming CHW-*g*-PCL(III) sheet as the representative of all the sheets.

TABLE II
DSC and DMA Data of the CHW-*g*-PCL Nanocomposites with Various PCL Content

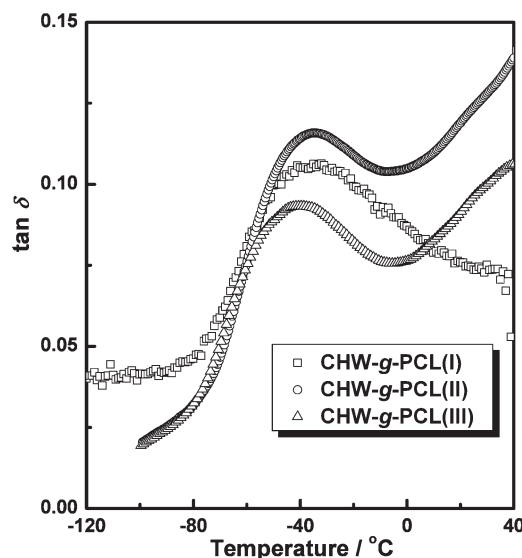| Sample | DSC data | | DMA Data | |
	T_m (°C)	ΔH_m (J g^{-1})	$T_{\alpha,max}$ (°C)	$H_{loss-peak}$
CHW-*g*-PCL(I)	57.10	64.88	−32.00	0.106
CHW-*g*-PCL(II)	56.06	65.22	−34.42	0.116
CHW-*g*-PCL(III)	56.48	64.63	−39.58	0.093

Figure 9 Loss factor (tan δ) as functions of temperature for the thermoforming CHW-g-PCL sheets with various CHW content.

occurrence of T_m and ΔH_m verified the presence of the crystalline fraction of grafted PCL chains. It was well-consistent with the XRD and FTIR results. DMA is a powerful technique to reflect the mobility of segment through α-relaxation at molecular-level, for which the specific heat increment of glass transition at domain-scale measured from DSC is generally ill-defined. As a result, the glass transition of PCL component, which was absent in DSC thermograms, was shown as α-relaxation determined by DMA. Table II also summarizes the α-relaxation temperature ($T_{\alpha,max}$) and height of loss-peak ($H_{loss-peak}$) of all the CHW-g-PCL nanocomposites from the tan $\delta - T$ curves (Fig. 9). Although the crystalline degree of grafted PCL chains increased with an increase of the PCL content in CHW-g-PCL (seen in the FTIR results), the $T_{\alpha,max}$s gradually shifted to low temperature. Such increasing freedom of motion was attributed to the decrease of rigid CHW content in CHW-g-PCL, namely the inhibition of CHW to the motion of PCL segment in amorphous region decreased.

CONCLUSIONS

The thermoformable bionanocomposites of chitin whisker-*graft*-polycaprolactone (CHW-*g*-PCL) were synthesized, and could be injection-molded as the sheets by virtue of long "plasticizing" PCL tails onto the CHW surface. The resultant materials showed a structure of cocontinuous phase mediated with the entanglement of grafted PCL chains. Except for the thermoformablility, the grafted PCL chains determined the mechanical and physical properties of nanocomposites as well. With an increase of the PCL

content in CHW-*g*-PCL, the strength and elongation as well as the hydrophobicity of the nanocomposites were simultaneously increased. Meanwhile, the entangling of grafted PCL chains facilitated the transferring of the stress to rigid CHW, and hence, fully played the reinforcing function of rigid CHW. To our knowledge, this is the first report of developing the thermoformable bionanocomposites based on polymer grafted natural nanocrystal. Moreover, such new bionanocomposite materials with high mechanical performances could be believed to have great potential applications.

References

1. Mecking, S. Angew Chem Int Eng 2004, 43, 1078.
2. Smith, R. Biodegradable Polymers for Industrial Applications, CRC Press: Cambridge, England, 2005.
3. Wool, R.; Sun, X. S. Bio-Based Polymers and Composites, Academic Press: Boston, Massachusetts, 2005.
4. Darder, M.; Aranda, P.; Ruiz-Hitzky, E. Adv Mater 2007, 19, 1309.
5. Yang, K. K.; Wang, X. L.; Wang. Y. Z. J. Ind Eng Chem 2007, 13, 485.
6. Azizi Samir, M. A. S.; Alloin, F.; Dufresne, A. Biomacromolecules 2005, 6, 612.
7. Paillet, M.; Dufresne, A. Macromolecules 2001, 34, 6527.
8. Putaux, J. L.; Molina-Boisseau, S.; Momaur, T.; Dufresne, A. Biomacromolecules 2003, 4, 1198.
9. Angellier, H.; Choisnard, L.; Molina-Boisseau, S.; Ozil, P.; Dufresne, A. Biomacromolecules 2004, 5, 1545.
10. Angellier, H.; Molina-Boisseau, S.; Dole, P.; Dufresne, A. Biomacromolecules 2006, 7, 531.
11. Angellier, H.; Molina-Boisseau, S.; Dufresne, A. Macromolecules 2005, 38, 9161.
12. Yuan, H.; Nishiyama, Y.; Wada, M.; Kuga, S. Biomacromolecules 2006, 7, 696.
13. Nait, K. G.; Dufresne, A. Biomacromolecules 2003, 4, 1835.
14. Angellier, H.; Molina-Boisseau, S.; Belgacem, M. N.; Dufresne, A. Langmuir 2005, 21, 2425.
15. Thielemans, W.; Belgacem, M. N.; Dufresne, A. Langmuir 2006, 22, 4904.
16. Labet, M.; Thielemans, W.; Dufresne, A. Biomacromolecules 2007, 8, 2916.
17. Song, S.; Wang, C.; Pan, Z.; Wang, X. J Appl Polym Sci 2008, 107, 418.
18. Gopalan Nair, K.; Dufresne, A. Biomacromolecules 2006, 4, 666.
19. Ljungberg, N.; Cavaillé, J. Y.; Heux, L. Polymer 2006, 47, 6285.
20. Ljungberg, N.; Bonini, C.; Bortolussi, F.; Boisson, C.; Heux, L.; Cavaillé, J. Y. Biomacromolecules 2005, 6, 2732.
21. Chazeau, L.; Cavaillé, J. Y.; Canova, G.; Dendievel, R.; Boutherin B. J Appl Polym Sci 1999, 71, 1797.
22. Garcia de Rodriguez, N. L.; Thielemans, W.; Dufresne, A. Cellulose 2006, 13, 261.
23. Chauve, G.; Heux, L.; Arouini, R.; Mazeau, K. Biomacromolecules 2005, 6, 2025.
24. Helbert, W.; Cavaillé, J. Y.; Dufresne, A. Polym Compos 1996, 17, 604.
25. Matos Ruiz, M.; Cavaillé, J. Y.; Dufresne, A.; Graillat, C.; Gerard, J. F.; Macromol Symp 2001, 169, 211.
26. Matos Ruiz, M.; Cavaillé, J. Y.; Dufresne, A.; Gerard, J. F.; Graillat, C. Compos Interfaces 2000, 7, 117.
27. Cavaillé, J. Y.; Dufresne, A.; Paillet, M.; Azizi Samir, M. A. S.; Alloin, F.; Sanchez, J. Y. Fr. Pat. FR2,841,255 (2002).

28. Cao, X.; Dong, H.; Li, C. M. Biomacromolecules 2007, 8, 899.

29. Chen, G. J.; Wei, M.; Chen, J. H.; Huang, J.; Dufresne, A.; Chang. P. R. Polymer 2008, 49, 1860.

30. Dufresne, A.; Kellerhals, M. B.; Witholt, B. Macromolecules 1999, 32, 7396.

31. Dufresne, A. Compos Interfaces 2003, 10, 369.

32. Kvien, I.; Tanem, B. S.; Oksman, K. Biomacromolecules 2005, 6, 3160.

33. Petersson, L.; Kvien, I.; Oksman, K. Compos Sci Technol 2007, 67, 2535.

34. Morin, A.; Dufresne, A. Macromolecules 2002, 35, 2190.

35. Noshiki, Y.; Nishiyama, Y.; Wada, M.; Kuga, S.; Magoshi, J. J Appl Polym Sci 2002, 86, 3425.

36. Lu, Y.; Weng, L.; Cao, X. Carbohydr Polym 2006, 63, 198.

37. Angles, M. N.; Dufresne, A. Macromolecules 2001, 34, 2921.

38. Lu, Y.; Weng, L.; Zhang, L. Biomacromolecules 2004, 5, 1046.

39. Wang, Y.; Cao, X.; Zhang, L. Macromol Biosci 2006, 6, 524.

40. Zheng, H.; Ai, F.; Chang, P. R.; Huang, J.; Dufresne, A. Polym Comps, DOI: 10.1002/pc.20612.

41. Nair, K. G.; Dufresne, A. Biomacromolecules 2003, 4, 657.

42. Yu, J.; Ai, F.; Dufresne, A.; Gao, S.; Huang, J.; Chang, P. R. Macromol Mater Eng 2008, 293, 763.